Automatic Verification of Camera, Radar, LIDAR Sensors Synchronization and Calibration for Automotive Applications

Gaweł Bartosik [1,2,*], Mateusz Komorkiewicz [1,3], Dariusz Marchewka [1,3], and Paweł Skruch [1,2]

[1] AI/ML Organisation, Aptiv Services Poland S.A., Kraków, Poland
[2] Faculty of Electrical Engineering, Automatics, Computer Science, and Biomedical Engineering, AGH University of Krakow, Kraków, Poland
[3] Center of Excellence in Artificial Intelligence, AGH University of Krakow, Kraków, Poland
Email: gawel.bartosik@aptiv.com (G.B.); mateusz.komorkiewicz@aptiv.com (M.K.); dariusz.marchewka@aptiv.com (D.M.); pawel.skruch@aptiv.com (P.S.)
*Corresponding author

***Abstract*—The development and verification of automotive perception systems require collecting data from various sensors mounted on a vehicle, such as cameras, radars, and Light Detection and Ranging sensors (LIDARs). It is not enough to simply record the data; maintaining proper calibration and synchronization between the sensors throughout the entire data recording process is crucial. This paper presents a device designed specifically to verify the calibration and synchronization of vehicle sensors, including LIDARs, radars, and cameras. The proposed solution utilizes a spinning disk that is precisely synchronized with an external clock signal, offering adjustable phase shifting and featuring permeable zones that act as shutters to trigger sensor activation. A cascade double-loop control system is implemented to minimize phase differences, ensuring high accuracy in synchronization. The quality of the synchronization mechanism was evaluated using an oscilloscope, with results showing a high level of precision. Finally, the device's effectiveness was validated through an experiment conducted on the target vehicle sensor system, confirming its efficiency in maintaining synchronization.**

***Keywords*—automotive, camera, Light Detection and Ranging (LIDAR), radar, calibration, synchronization, data recording**

I. Introduction

Today's automotive industry experiences a dynamic and important growth in sophistication and availability of automatized driving and assistance systems. Not only is there important development in autonomous vehicles, a significant expansion of classic Advanced Driver Assistance Systems (ADAS) takes place.

Functionalities can be of varying complexity, ranging from Adaptive Cruise Control, Lane Keeping Assist [1], through Driver Monitoring Systems [2] up to functions for autonomous driving, such as traffic light recognition [3] or freespace detection [4]. To fulfill needs of those systems vehicles are equipped with a variety of sensors such as radars [5], cameras, and Light Detection and Ranging sensors (LIDARs) in different configurations [6] (see Fig. 1). Furthermore, the development of vehicle ADAS systems requires the collection of large volumes of sensor data, which are essential for the development, verification, and validation of algorithms [7, 8].

Fig. 1. Typical data recording vehicle used during Advanced Driver Assistance Systems (ADAS) system development.

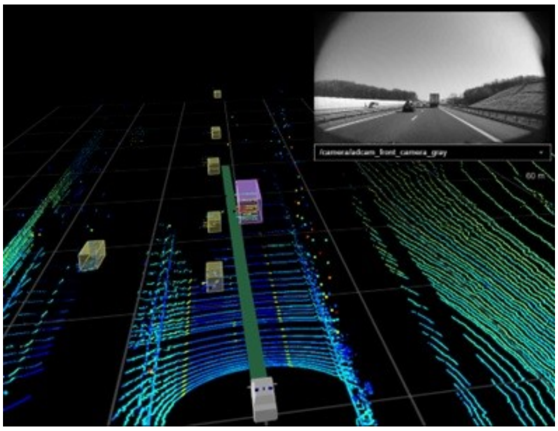

Fig. 2. Visualization of data from an automotive perception system includes camera images, Light Detection and Ranging (LIDAR) point clouds, radar detections, and bounding boxes for detected objects.

Manuscript received October 24, 2024; revised November 22, 2024; accepted February 12, 2025; published May 22, 2025.

One key challenge in making the data useful is ensuring sensor extrinsic calibration, which aligns different sensor readings to a common coordinate system. Another critical issue is maintaining proper sensor synchronization. Precise timing is crucial, as it allows all sensors to capture measurements simultaneously, enabling accurate object tracking and compensating for vehicle movement (see Fig. 2). Proper synchronization is essential for fusing object data from multiple sensors and for using LIDAR as a reference data source to label the environment and evaluate sensor performance [9].

So far there are several approaches to sensor synchronization:

- Sensors are not synchronized; data is time stamped by logger when it reaches the recording device.
- Sensors are synchronized to master clock (e.g., generic Precision Time Protocol (gPTP) or Global Positioning System Pulse Per Second (GPS PPS) [10]) and time stamp is embedded into data packets which are just collected by logger (see Fig. 3) [11].
- Sensors are synchronized online based on road and objects features, e.g., road curvature [12, 13].
- Mixtures of above, e.g., multiple loggers, special data probes adding timestamps etc.

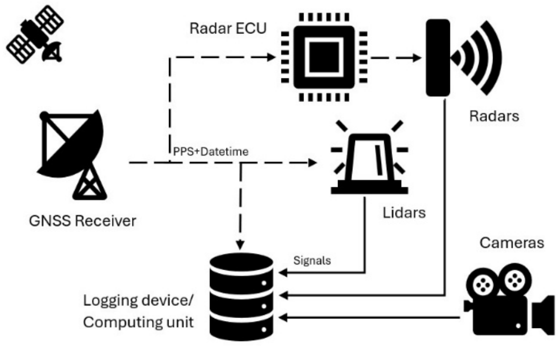

Fig. 3. Automotive perception system data logging and time stamping.

Ensuring synchronization signals for automotive sensors like radars and cameras is not a straightforward task. Radars can use an external trigger or a high-priority Controller Area Network (CAN) frame [14], while cameras rely on an imager trigger signal, which is complex to manage in automotive environments. Transitioning from gPTP or PPS domains to CAN frames requires specialized hardware. Additionally, sensor processing times introduce latency, which is difficult to control. As a result, assessing the quality of sensor synchronization becomes challenging. Even when there are discrepancies in object locations across sensor readings, it is unclear whether the issue stems from poor sensor synchronization (i.e., readings from different time frames) or sensor inaccuracies and transport latency.

A. Related Work

Spatial calibration of sensors is a broadly researched topic, Qiu *et al*. [15] provided a comprehensive review of the topic. Intensely researched is the software-only approach, that relies on data processing to detect miscalibrations. Such solution is presented by Peng *et al*. [16], which aims to assess the camera-lidar calibration, enabling real-time tweak of the parameters. Another idea, presented by Yan *et al*. [17], offers a ready to use open-source toolbox for online sensor-vehicle calibration. Kumar *et al*. [18] proposed a spatiotemporal calibration method for the most common sensor set—radar and camera. This set of sensors is being researched also, in e.g., transportation engineering: Du *et al*. [19] propose a method for radar-camera synchronization in roadside measurements. On the other side are hardware-based ideas; Apple in their patent [20] describes a mobile, vehicle-mounted solution that focuses exclusively on vision sensors. However, this solution cannot be applied to other sensor types, nor does it allow for synchronization verification. Toyota addressed the issue in their patent [21], but this solution has limited mobility and is restricted to position calibration only. Nvidia introduced another approach for multi-sensor alignment in their patent [22]. Their method utilizes the vehicle's sensors to identify object correspondences between different sensors, facilitating more accurate alignment.

Achieving temporal synchronization is the other challenge in multi sensor systems. Sommer et al. propose a low-cost hardware system for use with cameras and lidars, based on Raspberry Pi and PTP [23]. Similar systems, based on an Advanced RISC Machine (ARM) microprocessor boards are independently presented in [24, 25]. An FPGA based synchronization system is presented in [26]. A fully software solution based on Robot Operating System (ROS) is presented in [27]. Another approach to synchronizing cameras and radars is described in [12]. The paper introduces a method for time synchronization of radar and camera systems using least squares cubic spline curve fitting. Building on this synchronization, the paper proposes a rapid spatial joint calibration method for the radar and camera systems, utilizing the vehicle's longitudinal symmetry plane for alignment. Temporal synchronization of lidar sensors is a challenge not only in vehicles—Patel *et al*.'s [28] research machine learning based methods in devices aimed at helping visually impaired people navigate.

Works mentioned above concentrate on achieving and maintaining temporal synchronization of sensors. Much less researched is the topic of how to measure and validate synchronization quality. Yuan *et al*. [29] try to tackle this challenge in their article. The authors propose a method to convert and amplify small time deviations in synchronized multi-sensor systems into measurable physical quantities for more accurate calculation. The study evaluates two different time-synchronized multi-sensor systems, and the results provide detailed insights into their time synchronization accuracy levels. However, the solutions they describe are all workbench based and impossible to perform on sensors mounted on a vehicle, and they don't provide support for radars. To the best of our knowledge, no existing system simultaneously verifies the calibration and synchronization of all three primary automotive sensors—radar, camera, and LIDAR.

B. Contribution

To accurately assess sensor synchronization, we propose a dedicated synchronization unit designed to operate across the radar, LIDAR, and camera spectrums. This unit enables precise measurement and validation of both sensor synchronization and calibration.

Main original idea is a device, which camera, lidar, and radar triggering elements are mechanically constrained. Such concept guarantees perfect synchronization of the parts, generating reliable signal that can be used as ground-truth for measurements. Second part is to have the device synchronized to an external clock source, in this case GPS time signal, for a universal time reference. Third part is that we can use the same device for calibration verification—as the dimensions and offsets of sensor triggers are known.

II. System Description

The proposed device features a rotating disk synchronized with a GPS PPS signal, functioning as a shutter. The disk includes two types of zones: one acts as a planar mirror, reflecting both laser (infrared) and radar (microwave) signals, while the other is a slot that is transparent to radar and reflective to laser signals (Fig. 4). The reflective zone is also utilized for camera system detection. The mirror zone effectively deflects and dissipates signals upwards, making the device effectively invisible to LIDAR and radar. When aligned with the slot zone, however, the device generates strong and clear detections on both sensors. The disk's steady, GPS calibrated rotations produce a reliable digital signal of known frequency. Behind the mirror, a radar corner reflector [30] is positioned. The disk is angled so that the mirror zone disperses both radar and LIDAR signals upwards, rendering the device invisible to these sensors. Consequently, when the slot on the disk aligns with the upward position, it allows for reliable and accurate detections by the sensors (see Fig. 5).

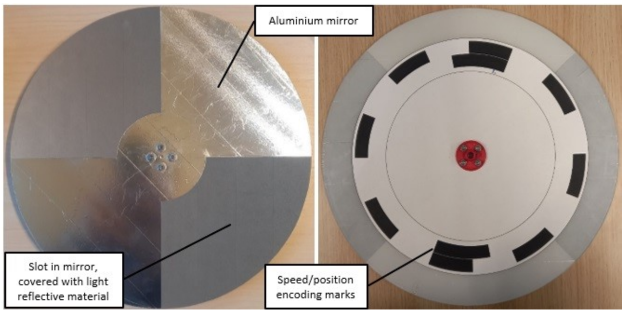

Fig. 4. Left picture: The disk's front side, displaying two types of zones: an aluminum mirror and a slot covered with a light-reflecting material. Right picture: The disk's reverse side, showing the position and speed encoding marks.

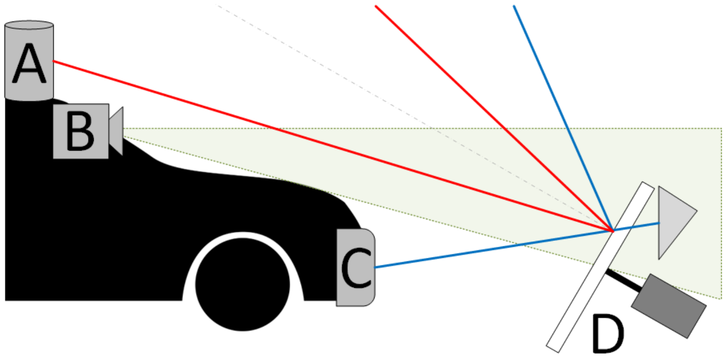

Fig. 5. Principle of signal reflection/dissipation by the shutter/mirror disk.
A—LIDAR, B—camera, C—radar, D—proposed device. Red—LIDAR beam; Blue—radar signal; Green—camera field of view.

The disk is driven by a BLDC (Brushless DC) motor and driver, which are managed by a microcontroller. The disk's rotation and position are precisely controlled using an encoding setup that includes two reflection sensors and black matte marks on the disk's reverse side. The first sensor synchronizes the disk's position with the GPS PPS signal and operates based on two marks aligned with the slot zone. The second sensor monitors and regulates the disk's revolutions. The motor is controlled through feedback from both the revolution and position readings. Additionally, a phase shift can be introduced to aid in sensor calibration. This setup provides a continuous usable shutter speed range of 4−100 Hz with a dual-zone disk (half mirror, half slot) and 2−50 Hz with a single-zone disk.

This design allows us to provide accurately synchronized triggers for all three sensors—radar, LIDAR, and camera. The location of the triggers is known, their displacement is identified and relatively small. This way it can be used for two elemental purposes simultaneously:

- Sensor synchronization verification
- Sensor position calibration verification

The device can be incorporated as a part of a bigger system; it can be, e.g., a part of an automatic synchronization and/or calibration verification tool, or a multi-device setup.

The complete control system for the verification device is presented in Fig. 6. It consists of three main parts:

1) Disk rotation speed control
2) GPS PPS signal synchronization
3) Disk position control.

Each control subsystem is described in more details in the next subsections.

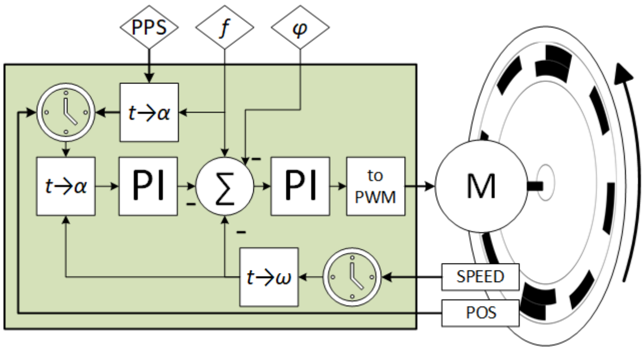

Fig. 6. Block diagram of device control system. Green field: microcontroller.
Inputs: PPS—pulse-per-second signal, e.g., from GNSS receiver; *f*—requested device frequency; *φ*—requested phase shift.

A. Disk Rotation Speed Control

The disc speed controller represents the final stage of the cascade control system, directly regulating the disc drive. It receives inputs from two sources: the desired rotation value set by the computer via the Universal Asynchronous Receiver/Transmitter (UART) bus, and the output of the position controller described in Section II.B. Additionally, it incorporates feedback from the measurement of the actual disc speed. The schematic diagram of this controller is shown in Fig. 7.

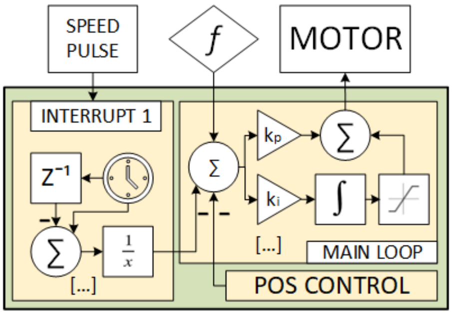

Fig. 7. Block diagram of the speed control subsystem. Inputs: SPEED PULSE—signal from speed sensor; *f*— requested device frequency.

The measurement of the rotational speed is carried out by measuring the time between successive interruptions from the reflective speed sensor. This time is converted to the rotational speed expressed in hertz according to the formula:

$$f = \frac{1}{\Delta_t \cdot n} \tag{1}$$

where f denotes the speed (in Hz), Δt is the time difference between successive pulses from the reflective speed sensor (in seconds), n is the number of markers in a full rotation of the disk.

Due to the applied measuring system (reflective sensor and a marked disk), the obtained values are characterized by high noise, especially of an impulsive nature (so-called spikes). It introduces significant difficulty in controlling the system and creates a risk of the control system destabilization. To prevent this, two-stage filtration was used:

1) Single dimension median filter (window length of 7 samples),
2) Low pass filter.

Speed control is performed in a closed feedback loop using a PI controller. Integral part turned out to be necessary to remove a constant control error. Tuning constraints k_p are k_i were selected experimentally to remove constant error and limit the oscillations in the steady state. The parameters are presented in Table I.

TABLE I. EXPERIMENTALLY OBTAINED TUNING PARAMETERS FOR PI REGULATOR

Controller	k_p	k_i	max_i
Speed controller	8.0	0.008	±500
Position controller	2.5	0.001	±10000

k_p: Tuning constraints for proportional action
k_i: Tuning constraints for integral action
max_i: Limit value for the integral part (*anti-windup*)

B. Disk Position Control

The disc position controller is the first element of the cascade control system of the device. It is a high-level software implementation of a Phase-Locked Loop (PLL). Its operation is limited to the situation in which the speed error value is sufficiently low. The input to the controller is the position error, measured using a reference signal and information from the position sensor. The output from the controller introduces a correction to the speed settings in the second stage of the controller responsible for speed (described in Section II.A). The schematic diagram is in Fig. 8.

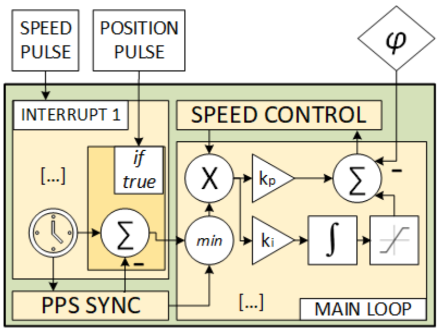

Fig. 8. Block diagram of position control subsystem.
Inputs: *φ*—requested phase shift.

1) Measuring the disc position error: During each interrupt phase for the reflective speed sensor, the state of the position sensor is checked. If it is high, the time difference between the last pulse from the reference signal generator and the occurrence of the interrupt from the reflective sensor is calculated. This difference is with a positive sign. In parallel, during each pulse from the reference generator, the same time difference is calculated, in this case it is with a negative sign. For further calculations, the difference with the smaller absolute value is always used. The disc position error is calculated according to the formula:

$$e_{pos} = \begin{cases} \Delta_{t_1-t_2} \cdot f & \text{if } \Delta_{t_1-t_2} < \Delta_{t_2-t_1} \\ -\Delta_{t_2-t_1} \cdot f & \text{if } \Delta_{t_1-t_2} > \Delta_{t_2-t_1} \end{cases} \quad (2)$$

2) Position regulator: Position control is performed in a closed feedback loop using a PI controller. The controller output is summed with the input of the position control system, realizing a cascade control system. The use of the integral part was necessary to eliminate the constant error. The parameters are given in Table I.

C. Synchronization with PPS Reference Signal

To synchronize the disk rotation with PPS signal the error between disk position and some reference needs to be measured. The problem is that PPS signal cannot be used directly because it has a constant frequency of 1Hz. The solution is to use the PPS signal to generate new reference with desired higher frequency which can be used to compare with disk rotations. To achieve this goal, a reference signal generator was created. The block diagram of this unit is presented in Fig. 9.

Based on the microcontroller timer unit a 100 kHz clock was configured. It is later modified by adjustable frequency divider to generate the reference signal which frequency is equal to the disk rotation frequency. At the same time, the PPS signal is closely monitored and used for internal microcontroller latencies adjustment which might otherwise influence the 100 kHz clock.

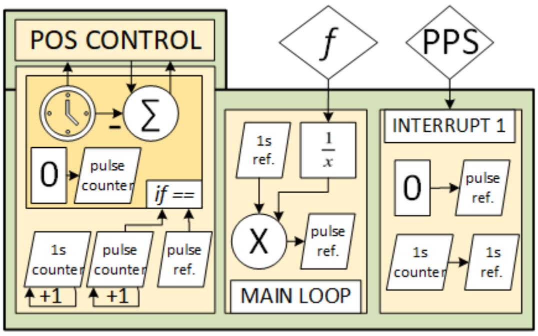

Fig. 9. Block diagram of the synchronization block with PPS. Inputs: *f*—requested device frequency, PPS—pulse-per-second signal.

III. Prototype

The final prototype of the device is shown in Fig. 10. It represents the culmination of numerous design iterations and evolutionary improvements. To ensure the device remains invisible to radar radiation, standard aluminum profiles could not be used. Instead, hardwood plywood was selected as the primary material. However, in future iterations of the project, the use of polymer components should be considered to potentially enhance performance and durability.

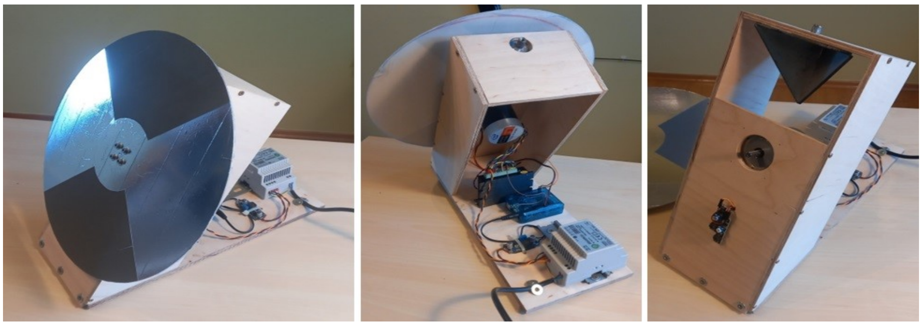

Fig. 10. Prototype of the device Left: shutter disk; Center: motor and logic device; Right: microwave corner reflector mounted on the top panel.

The aperture disc is a critical component of the device. It is crafted from clear polystyrene plate due to its non-metallic nature, ease of processing, low weight, high strength, and wide availability. The plate is divided into four equal sections, with one pair of sections being permeable and the other pair serving as mirrors. The disc is mounted on the motor shaft using a specially designed clutch, which was produced using FDM/FFF 3D printing technology.

IV. Experiments

To verify the device's functionality and ensure that the intended parameters were met, two types of tests were conducted. The first test, performed on a test bench using an oscilloscope with statistical measurements, aimed to quantify the synchronization quality and signal stability of the device—crucial factors to consider signal generated by it as "ground truth" for synchronization verification. Details of the methodology and results are provided in Section V. The second test involved evaluating the device with a vehicle equipped with LIDAR and radar sensors. This was needed to prove that the appliance triggers vehicle's sensors correctly in a distinguishable manner, as well as to present how the calibration verification can be performed. This test is described in Section VI.

V. Measurement of PPS Signal Synchronization and Signal Stability

The first test that was performed consisted of measuring the time difference between the rising edge of the PPS signal and the rising edge of the signal from the reflective sensor responsible for the disc position (Fig. 11). The measurement was performed in a statistical manner—that is, the average value of the time difference and its standard deviation were determined, of which 30 were performed for each measurement point. The period and standard deviation of the period value were also measured, as an indicator of the device's speed stability. The functions built into the oscilloscope were used to perform these measurements and calculations. 25 points were determined for the 10 Hz speed by introducing successive phase shifts of 15°, and 13 measurement points for the 20 Hz speed with shifts of 30°.

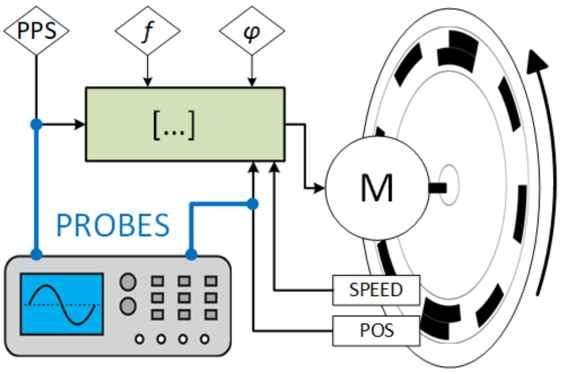

Fig. 11. Measurement system setup.

To assess the measured values a quality metric was introduced. As the device is designated to work with automotive systems, a real-life scenario was used as a basis for it. The assumption is, the perception system of a car should have a less than 1cm distortion, even with highway speeds. Thus, if the velocity is assumed to be 120km/h, that results in a 0.3 ms of sensor missynchronization. This will be the maximum value of the measured offset from ideal time.

The test stand consists of the tested device and a Siglent 1102X dual-channel oscilloscope. The diagram of the measurement system is in Fig. 11. The oscilloscope was configured to collect statistical measurements, from which the selected measurement was the period of the signal T on channel 2 (signal from the reflective sensor for position) and the time difference measurement t_{real} between the rising edges of the signals on channel 1 (PPS signal) and 2 (signal from the reflective sensor for position). Statistical measurement on this device returns the values:

- last measured value,
- highest measured value,
- lowest measured value,
- average of all measurements,
- standard deviation of all measurements.

The test, for a given speed, proceeds as follows:

1) Speed assignment,
2) Phase shift assignment,
3) Waiting for stability,
4) Starting the measurement,
5) After obtaining 30 samples, stop further measurements,
6) Saving the measurement results,
7) Go to the next measurement point, repeat steps 2–6
8) After completing the series of measurements, go to the next speed—return to step 1.

The results are presented in Fig. 12 (for 10 Hz) and Fig. 13 (for 20 Hz), where α_{req} [°] is the amount of set phase shift from signal 2 to 1, Δt [ms] is calculated difference between the target and actual time value of the second to first signal shift.

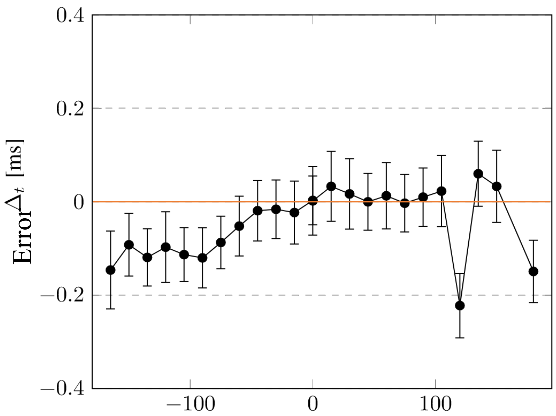

Fig. 12. Synchronization error vs. forced phase shift graph—measurements for 10Hz signal. The expected value is 0.

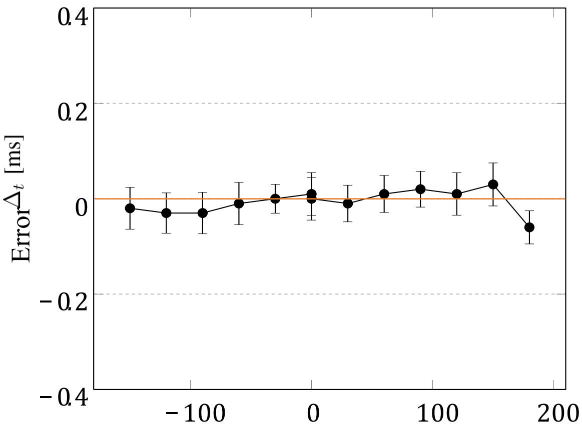

Fig. 13. Synchronization error vs. forced phase shift graph—measurements for 20 Hz signal. The expected value is 0.

Based on the conducted experiments, it can be concluded that the maximum value of the offset error is −0.22 ms with a standard deviation of 138.1 µs, while most of the measurements are in a much smaller range. All these values are below the limit of ±0.3 ms specified as the maximum value for this quality metric.

VI. IN THE CAR TESTS

After proving the performance of the device by measuring synchronization accuracy with GPS signal, the next step was to test it with real automotive sensors. The tests were carried out using a vehicle equipped with the following sensors (Fig. 1):

1) LIDAR Hesai Pandora—mounted on the roof, centrally—nominal refresh rate 10 Hz, sensor synchronization using PPS signal supplied directly from the GPS receiver [31],

2) 2x Mid-range radar—mounted in the front and rear bumpers of the car—nominal refresh rate 20 Hz, sensor synchronization using time data sent via CAN bus via a special "NMEA+PPS-to-CAN" system [14],
3) 4x Mid-range radar [32]—mounted on the corners of the vehicle—nominal refresh rate 20 Hz, sensor synchronization using time data sent via CAN bus via a special "NMEA+PPS-to-CAN" system,
4) GNSS NovAtel PwrPak7—GPS, Galileo, Glonass and IMU sensors, allowing precise vehicle location and time synchronization.

A. *Initial Observations*

The test stand was prepared according to the diagram in Fig. 4. From the software architecture point of view, the ROS—Robot Operating System [33] was used. Each sensor has its own ROS node enabling both the real time preview in RViz visualization tool as well as recording of data topics with the rosbag logging feature.

The following methodology was used to perform the experiments:

- Recordings for two speeds: 10 and 20 Hz,
- For each speed, 25 recordings with phase shifts at 15° intervals covering a full rotation of 360°,
- Each recording 20 s long,
- Two additional recordings for the static disk in positions 1 and 0.

In total, 60 ROSBAG files with a total capacity of 69.6 GB were recorded as part of the study. Example visualizations of this data are shown in Fig. 14.

Based on the observation of data visualization in the RViz program (Fig. 14) conducted during data collection, the following observations can be made:

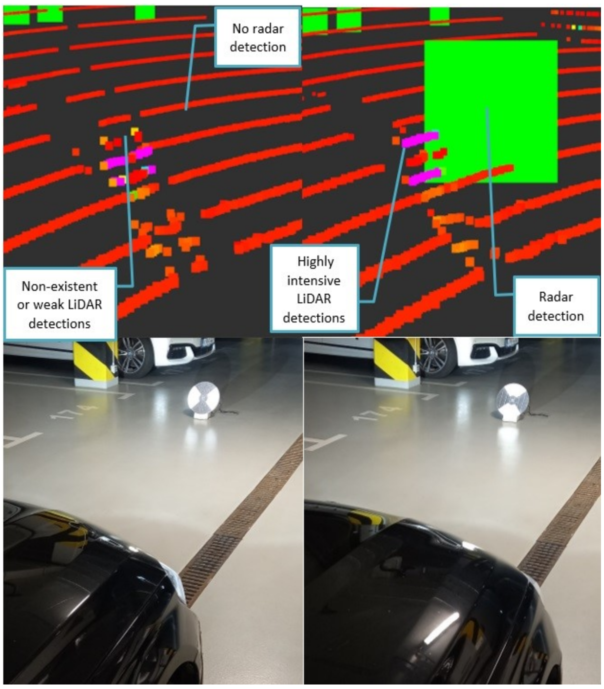

Fig. 14. Visualization of operation. Left: Device is invisible to sensors, mirror deflects signals; Right: Device reflects signal back to sensors, causing detections

- The LIDAR pointcloud is always reflecting on the disk, but the reflection intensity can be used to automatize the determination of disk position.
- Radar corner reflector and shuttering mechanism is working as expected, the position and state can be determined directly by existence of radar detection.
- Camera is also according to expectation; the disk position is possible to be determined.

Also, some further observations could be made regarding the sensor setup in the vehicle used for tests:

- LIDAR operates at a synchronized frequency of 10 Hz, and the location where the synchronization test device was set was detected with a shift of about +90°.
- The forward radar operates at a frequency unsynchronized with PPS other than 20 Hz, which causes a full transition of the phase shift of 0° → 180° → 360° (0°) in about 10 min.
- Sensor calibration: as seen on Fig. 15 it is possible to see how the device can be used for calibration verification. On this figure it is visible how the representation of the device is offset between radar and lidar. In this example, the sensors are offset by ca. 44 cm (calculated using RViz measure tool). The real distance between the trigger elements is less than 10 cm longitudinally.

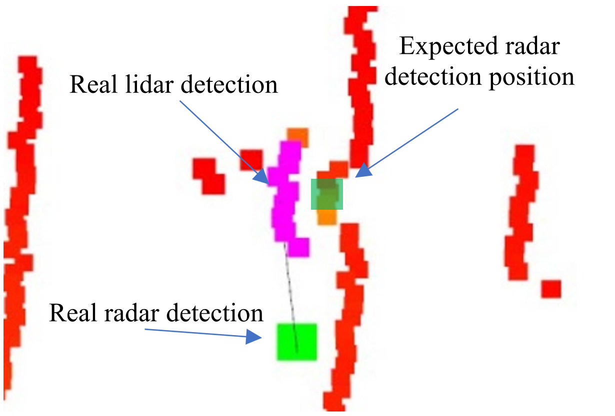

Fig. 15. Bird eye view of combined lidar and radar pointcloud. Visible calibration issue, shown using the device. Green (radar signal) and purple points (lidar signal) should be overlapping. Instead, a distance of ca. 44 cm is present.

The results prove that the proposed device can properly stimulate the sensors in the vehicle.

VII. Conclusions

The synchronization device described in this article plays a crucial role in sensor calibration and validation processes for vehicle systems. It verifies the calibration and synchronization of LIDAR, radar and camera sensors, validates vehicle setups after initial deployment, and ensures system accuracy before data logging tasks. Its versatility improves the efficiency and reliability of sensor systems across various operational scenarios, including data logging campaigns and end-of-line factory verification. The device could be incorporated in a bigger, scalable system consisting of multiple units, which with use of data streams from tested sensors and purpose built algorithms, could automatically perform validation tasks, calculate the time offsets and calibration misalignments.

Future work could consist of automatization by the use of algorithms, performing experiments with multiple units, 360° around the car sensor verification tasks, refining the prototype using better materials, adding another sensor domain to the stack (e.g., ultrasound sensors). A promising direction would be to design a ROS module which could calculate the sync and calibration offsets—which could then be easily used to compensate the setup.

Conflict of Interest

The authors declare no conflict of interest.

Author Contributions

All four authors co-wrote the paper; GB designed and manufactured the prototype, sourced and processed the data; MK defined the problem, researched possible design solutions, made literature review; DM made literature review; PS directed the scientific work, verified the data. All authors had approved the final version.

Funding

This work presents some results from the project titled "Development of innovative technologies in the field of active safety, which will be used in Advanced Driver Assistance Systems (ADAS) and autonomous driving systems intended for mass production", which has received funding from the European Union's Smart Growth Operational Programme 2014–2020.

References

[1] R. Bosch, *Safety, Comfort and Convenience Systems*, Bentley Publishers, 2006.

[2] Y. Dong, Z. Hu, K. Uchimura, and N. Murayama, "Driver inattention monitoring system for intelligent vehicles: A review," *IEEE Transactions on Intelligent Transportation Systems*, vol. 12, no. 2, pp. 596–614, June 2011. doi: 10.1109/TITS.2010.2092770

[3] M. Lee, J. Pyo, S. Bae, S. Joo, and T. Kuc, "Traffic light recognition for autonomous driving vehicle: Using mono camera and ITS," *Journal of Image and Graphics*, 2022.

[4] A. Popov, P. Gebhardt, K. Chen, and R. Oldja, "NVRadarNet: Real-time radar obstacle and free space detection for autonomous driving," in *Proc. 2023 IEEE International Conference on Robotics and Automation (ICRA)*, London, United Kingdom, 2023, pp. 6958–6964. doi: 10.1109/ICRA48891.2023.10160592

[5] M. Markel. (2022). *Radar for Fully Autonomous Driving*. Artech House. [Online]. Available: https://books.google.pl/books?id=nOF8EAAAQBAJ

[6] H. Sjafrie. (2019). *Introduction to Self-Driving Vehicle Technology*. Chapman & Hall/CRC Artificial Intelligence and Robotics Series. CRC Press. [Online]. Available: https://books.google.pl/books?id=B33ADwAAQBAJ

[7] M. Komorkiewicz *et al*., "Intelligent data handling in current and next-generation automated vehicle development—A review," *IEEE Access*, vol. 11, pp. 32061–32072, 2023. doi: 10.1109/ACCESS.2023.3258623

[8] E. Ghiasi, G. Ghajari, M. Gottipati, P. S. S. Gogineni, R. Galla, and N. Bourbakis, "Association of multi-sensor data for autonomous car driving: A comparative evaluation," in *Proc. 2024 IEEE 36th International Conference on Tools with Artificial Intelligence (ICTAI)*, Herndon, VA, USA, 2024, pp. 427–436. doi: 10.1109/ICTAI62512.2024.00068

[9] M. Szelest, W. Uzdrzychowski, and D. Grzechca, "GNU radio and USRP2 as a universal platform for verification of wireless communication devices used in automotive applications," in *Proc. the 19th International Conference Mixed Design of Integrated Circuits and Systems, MIXDES 2012*, 2012, pp. 436–440.

[10] Pentagon Office of the Department of Defense. *Global Positioning System—Standard Positioning Service. Performance Standard*. [Online]. Available: https://www.gps.gov/technical/ps/2020-SPS-performance-standard.pdf

[11] M. Faizullin, A. Kornilova, and G. Ferrer, "Open-source LiDAR time synchronization system by mimicking GNSS-clock," in *Proc. 2022 IEEE International Symposium on Precision Clock Synchronization for Measurement, Control, and Communication (ISPCS)*, Vienna, Austria, 2022, pp. 1–5. doi: 10.1109/ISPCS55791.2022.9918446

[12] S. Song *et al*., "Research on time synchronization and spatial calibration algorithms of radar and camera," *Journal of Physics: Conference Series*, 012044, Feb. 2023. doi: 10.1088/1742-6596/2428/1/012044

[13] K. Yuan, L. Ding, M. Abdelfattah, and Z. J. Wang, "LiCaS3: A simple LiDAR–camera self-supervised synchronization method," *IEEE Transactions on Robotics*, vol. 38, no. 5, pp. 3203–3218, Oct. 2022. doi: 10.1109/TRO.2022.3167455

[14] S. Corrigan. (August 2002). Introduction to the Controller Area Network (CAN). [Online]. Available: https://www.ti.com/lit/an/sloa101b/ sloa101b.pdf

[15] Z. Qiu, J. Martínez-Sánchez, P. Arias-Sánchez, and R. Rashdi, "External multi-modal imaging sensor calibration for sensor fusion: A review," *Information Fusion*, vol. 97, 101806, 2023. doi: 10.1016/j.inffus.2023.101806

[16] P. Peng, D. Pi, G. Yin *et al*., "Automatic miscalibration detection and correction of LiDAR and camera using motion cues," *Chin. J. Mech. Eng.*, vol. 37, no. 50, 2024. https://doi.org/10.1186/s10033-024-01035-3

[17] G. Yan, Z. Luo, Z. Liu, Y. Li, B. Shi, and K. Zhang, "SensorX2Vehicle: Online sensors-to-vehicle rotation calibration methods in road scenarios," *IEEE Robotics and Automation Letters*, vol. 9, no. 4, pp. 3775–3782, April 2024. doi: 10.1109/LRA.2024.3371261

[18] N. Kumar, A. Dasgupta, V. S. Mutnuri, and R. Pachamuthu, "An efficient approach for calibration of automotive radar–camera with real-time projection of multimodal data," *IEEE Transactions on Radar Systems*, vol. 2, pp. 573–582, 2024. doi: 10.1109/TRS.2024.3408231

[19] Y. Du, B. Qin, C. Zhao, Y. Zhu, J. Cao, and Y. Ji, "A novel spatio-temporal synchronization method of roadside asynchronous MMW radar-camera for sensor fusion," *IEEE Transactions on Intelligent Transportation Systems*, vol. 23, no. 11, pp. 22278–22289, Nov. 2022. doi: 10.1109/TITS.2021.3119079

[20] M. P. Kalscheur, Multi-sensor real-time alignment and calibration, US Patent 10788316, Sept. 2020.

[21] B. J. Pinkelman, T. Muck, and D. Prokhorov, Sensor calibration enclosures and methods of using sensor calibration enclosures to calibrate vehicle sensors, US Patent 11029179, June 2021.

[22] M. D. Wheeler and L. Yang, Calibrating sensors mounted on an autonomous vehicle, US Patent 10436885, Oct. 2019.

[23] H. Sommer, R. Khanna, I. Gilitschenski, Z. Taylor, R. Siegwart, and J. Nieto, "A low-cost system for high-rate, high-accuracy temporal calibration for LIDARs and cameras," in *Proc. 2017 IEEE/RSJ International Conference on Intelligent Robots and Systems (IROS)*, Vancouver, BC, Canada, 2017, pp. 2219–2226. doi: 10.1109/IROS.2017.8206042

[24] Y. Wang *et al*., "Hardware-based time synchronization for a multi-sensor system," in *Proc. 2024 IEEE/RSJ International Conference on Intelligent Robots and Systems (IROS)*, Abu Dhabi, United Arab Emirates, 2024, pp. 4600–4607. doi: 10.1109/IROS58592.2024.10802693

[25] X. Wu, H. Sun, R. Wu, and Z. Fang, "EverySync: An open hardware time synchronization sensor suite for common sensors in SLAM," in *Proc. 2024 IEEE/RSJ International Conference on Intelligent Robots and Systems (IROS)*, Abu Dhabi, United Arab Emirates, 2024, pp. 12587–12593. doi: 10.1109/IROS58592.2024.10801968

[26] S. Liu *et al*., "Brief industry paper: the matter of time—A general and efficient system for precise sensor synchronization in robotic computing," in *Proc. 2021 IEEE 27th Real-Time and Embedded Technology and Applications Symposium (RTAS)*, Nashville, TN, USA, 2021, pp. 413–416. doi: 10.1109/RTAS52030.2021.00040

[27] H. Hu, J. Wu, and Z. Xiong, "A soft time synchronization framework for multi-sensors in autonomous localization and navigation," in *Proc. 2018 IEEE/ASME International Conference on Advanced Intelligent Mechatronics (AIM)*, Auckland, New Zealand, 2018, pp. 694–699. doi: 10.1109/AIM.2018.8452384

[28] I. Patel, M. Kulkarni, and N. Mehendale, "Machine learning-based sensor synchronization for enhanced spatial awareness in assistive technologies," in *Proc. 2024 International Conference on Intelligent Systems and Advanced Applications (ICISAA)*, Pune, India, 2024, pp. 1–6. doi: 10.1109/ICISAA62385.2024.10829046

[29] S. Yuan *et al*., "Time synchronization accuracy verification for multi-sensor system," in *Proc. 2021 International Conference on Artificial Intelligence, Big Data and Algorithms (CAIBDA)*, 2021, pp. 21–24. doi: 10. 1109/CAIBDA53561.2021.00012

[30] C. Wolff. *Corner Reflectors—RadarTutorial.eu*. [Online]. Available: https://www.radartutorial.eu/17.bauteile/bt47.en.html

[31] Hesai Photonics Technology Co., Ltd. (2018). *Pandora All-in-One Sensing Solution for Autonomous Driving User's Manual*. [Online]. Available: https://www.manualslib.com/manual/1987296/Hesai-Pandora.html

[32] Aptiv. *Advanced Radars*. [Online]. Available: https://www.aptiv.com/en/solutions/advanced-safety/adas/radars

[33] Open Robotics. *Robot Operating System*. [Online]. Available: https://www.ros.org/